Results in Physics 65 (2024) 107991

Contents lists available at ScienceDirect

Results in Physics

journal homepage: www.elsevier.com/locate/rinp

Self-induced Bose glass phase in quantum quasicrystals

M. Grossklags [a], M. Ciardi [b,c,d], V. Zampronio [b,e], F. Cinti [b,c,f], A. Mendoza-Coto [a,g,*]

[a] Departamento de Física, Universidade Federal de Santa Catarina, 88040-900 Florianópolis, Brazil
[b] Dipartimento di Fisica e Astronomia, Università di Firenze, I-50019, Sesto Fiorentino (FI), Italy
[c] INFN, Sezione di Firenze, I-50019, Sesto Fiorentino (FI), Italy
[d] Institute for Theoretical Physics, TU Wien, Wiedner Hauptstraße 8-10/136, 1040 Vienna, Austria
[e] Departamento de Física Teórica e Experimental, Universidade Federal do Rio Grande do Norte, Brazil
[f] Department of Physics, University of Johannesburg, P.O. Box 524, Auckland Park 2006, South Africa
[g] Max Planck Institute for the Physics of Complex Systems, Nothnitzerstr. 38, 01187 Dresden, Germany

ARTICLE INFO

Keywords:
Quantum quasicrystals
Super quasicrystals
Bose glass phase
Long range order

ABSTRACT

We study the emergence of Bose glass phases in self sustained bosonic quasicrystals induced by a pair interaction between particles of Lifshitz–Petrich type. By using a mean-field variational method designed in momentum space as well as Gross–Pitaevskii simulations we determine the phase diagram of the model. The study of the local and global superfluid fraction allows the identification of supersolid, super quasicrystal, Bose glass and insulating phases. The Bose glass phase emerges as a quasicrystal phase in which the global superfluidity is essentially zero, while the local superfluidity remains finite in certain ring structures of the quasicrystalline pattern. Furthermore, we perform continuous space Path Integral Monte Carlo simulations for a case in which the interaction between particles stabilizes a quasicrystal phase. Our results show that as the strength of the interaction between particles is increased the system undergoes a sequence of states consistent with the super quasicrystal, Bose glass, and quasicrystal insulator thermodynamic phases.

Introduction

Physical systems forming self assembled patterns are ubiquitous in nature [1,2]. These patterns are usually produced by an effective interaction between the many constituents of an ensemble presenting some sort of competition [3–6]. The plethora of available frustrated interactions that naturally occur, or that can even be artificially engineered, combined with features like temperature, density of particles, defects or disorder, are responsible for the distinctive pattern formation observed in systems like supersolids [7–13], quantum cluster crystals [14,15], vortex lattices [16–19], Bose glasses [20–25], cavity QED mediated solids [26–31], among many others [32–36].

Generally, the most common scenario is the stabilization of some sort of periodic pattern at low temperatures while homogeneous states prevail in the high-temperature regime. Additionally, in the presence of a strong disorder or high concentration of system defects, even the low-temperature phase becomes disordered [20,37]. In this context, an exotic realization of pattern formation lying between an ordered and a disordered phase is the so-called quasicrystals [38,39]. These are ordered patterns that do not break translational symmetry but display a long-range orientational order whose symmetry is forbidden to any other periodic crystal in that specific dimension [40]. Such properties are the ultimate result of building a pattern with a wave vector basis whose dimension is higher than the dimension of the system.

In the context of soft matter physics, extensive work has been done on characterizing quasicrystal structures formed by many particles, namely, cluster quasicrystals [41–43]. In a foundational work by Barkan et al. [44], it was shown that cluster quasicrystals can be stabilized by an effective pair potential containing two properly selected competing length scales in the presence of moderate thermal fluctuations. In the quantum case, a recent work [45] has shown that to obtain a dodecagonal quasicrystal density pattern in a Bose–Einstein condensate, analog to the classical case but stabilized by quantum

* Corresponding author at: Departamento de Física, Universidade Federal de Santa Catarina, 88040-900 Florianópolis, Brazil.
E-mail addresses: matheus.grossklags@posgrad.ufsc.br (M. Grossklags), matteo.ciardi@tuwien.ac.at (M. Ciardi), vzampronio@fisica.ufrn.br (V. Zampronio), fabio.cinti@unifi.it (F. Cinti), alejandro.mendoza@ufsc.br (A. Mendoza-Coto).

[1] We have considered LPG interaction potentials with two minima and performed an analysis using the variational mean-field method and GPE simulations and verified that the cases in which the dodecagonal quasicrystal corresponds to the ground state of the system are located at moderate or high values of $\lambda^2\rho U$. We have observed that for some regions in this parameter space, the GPE simulations show that for a dodecagonal quasicrystal initial condition, the system evolves preserving the pattern but its stationary state does not correspond to the lowest energy configuration. This implies meta stability of the structure in the aforementioned cases. In this sense, the definitive criterion to determine the ground state is the value of the energy per particle of the system.

https://doi.org/10.1016/j.rinp.2024.107991
Received 12 March 2024; Received in revised form 7 August 2024; Accepted 22 September 2024
Available online 28 September 2024

fluctuations, three local minima must be correctly positioned in the Fourier transform of the effective pair interaction potential. To the best of our knowledge, potentials with two competing length scales could only stabilize quasicrystals in the regime of moderate to low intensity of quantum fluctuations.[1]

More recently, a number of publications [46–48] motivated by experimental feasibility have considered the stabilization of quasicrystal phases by the application of an external quasiperiodic potential in systems in which particles repel each other by contact interactions. One of the main results of these studies is the prediction of a Bose glass (BG) phase in such models. The well-established BG phase usually occurs as an intermediate phase between the Mott insulator state and the superfluid one. It appears in models of interacting bosons in the presence of some sort of disorder [20], and, recently, it has been also observed in two-dimensional quasicrystalline lattices [49]. In terms of its physical properties, it is a compressible insulator that hosts localized superfluid regions [50]. Due to the fact that the loss of coherence leading to the insulating behavior is a consequence of the lack of periodicity in the system, it is expected for the energy spectrum to manifest some sort of fractal structure, instead of energy bands as in the case of systems subjected to periodic external potentials [37,46,47]. In the described scenario, an intriguing possibility is the existence of a BG phase for quantum self-assembled quasicrystals in Bose–Einstein condensates at zero temperature.

In terms of experimental perspectives, it is important to mention that although we consider a specific mathematical form of the pair interaction potential, the main ingredient causing the physical behavior reported is the existence of a properly constructed three minima structure in its Fourier transform. The achievement of sign-changing interaction potentials in real space is the fundamental feature to generate the necessary frustration to stabilize quantum cluster quasicrystals and other exotic modulated states. In a number of recent works, effective interactions of this type mediated by photons in cavity QED systems have been used to produce different modulated patterns in ultra-cold quantum gases [26–31].

In this paper, we study the emergence of a self-organized BG phase in a Bose–Einstein quasicrystal condensate stabilized by the simultaneous role of quantum delocalization and a two-body interaction with multiple characteristic length scales. The BG phase is identified by studying simultaneously the local and global superfluidity since in our case the system is intrinsically compressible in all regimes of parameters. The ground state phase diagram of the system is studied using two complementary techniques, a variational approach [45] devised in momentum space, free of the effects of finite system sizes as well as periodic boundary conditions and the more standard Gross–Pitaevskii equation (GPE) simulations [51,52], as a secondary test for the precision of the main analytical method. Additionally, we perform continuous space Path Integral Monte Carlo (PIMC) simulations [53,54] for a finite portion of the system subjected to a confining potential in order to mimic possible experiments. The computational results for the finite system confirm qualitatively the main findings of the analytical study for the system in the thermodynamic limit.

The paper is organized as follows: Section "Model and approach" aims to introduce the model we studied as well as the analytical approach employed. Later, Section "Phase diagram" is going to describe the main outcomes which are condensed into a phase diagram. Section "PIMC simulations" is devoted to explore the systems thought using a PIMC numerical methodology. Finally, in Section "Conclusions and discussion" we discuss the achieved results and draw some conclusion.

Model and approach

We consider a two-dimensional system of N bosonic atoms of mass m at zero temperature. The particles interact through an isotropic

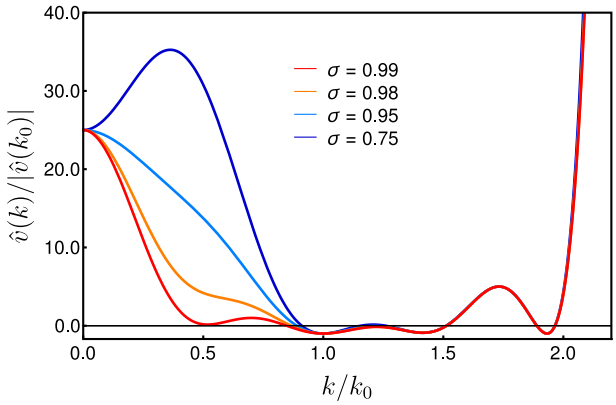

Fig. 1. Pair interaction potential $\hat{v}(k)$ for four different values of the parameter σ considered in the phase diagram of our model.

Lifshitz–Petrich–Gaussian [44] (LPG) pair interaction potential defined in momentum space as

$$\hat{v}(k) = Ve^{-k^2\sigma^2}\sum_{n=0}^{8} d_n k^{2n}. \tag{1}$$

This kind of pair interaction potential was originally proposed due to mathematical convenience to study models that stabilize periodic and aperiodic patterns in soft matter systems [44]. However, advances in experimental techniques now allow the production of sign changing effective interactions with a high degree of customization [26–31]. This is the main ingredient for the eventual engineering of an effective pair interaction potential $\hat{v}(k)$ with the minima structure considered in this work. We set the coefficients d_n in our model such that $\hat{v}(k)$ has a three minima structure. Two of these minima, at k_0 and $\sqrt{2+\sqrt{3}}k_0$, are degenerate, and a third one at $\sqrt{2}k_0$, is included to enhance the stability of the dodecagonal quasicrystal phase presented by this model in certain regions of the parameter space [45]. The resulting minima structure in Fourier space determines the values of the polynomial coefficients d_n associated with the LPG potential in Eq. (1), whereas σ assumes the role of the free parameter in our model. The range of values for the free parameter σ is obtained by requiring that the resulting potential maintains its global minimum at $k/k_0 = 1$. In Fig. 1, we show the family of potentials considered in the present work, the numerical expression of $\hat{v}(k)$ is obtained fixing the values of this function at $\{0, k_0, \sqrt{2}k_0, \sqrt{3}k_0, \sqrt{3+\sqrt{2}}k_0\}$ as well as the parameter σ.

In the limit of weak interactions, after expressing the spatial coordinates and the energy of the system in units of $\lambda = 2\pi/k_0$ and $\epsilon = \hbar^2/m\lambda^2$, respectively, we can write the energy per particle of the condensate as

$$\frac{E}{N} = \frac{1}{2}\int \frac{d^2\boldsymbol{x}}{A}|\boldsymbol{\nabla}\psi(\boldsymbol{x})|^2 + \frac{\lambda^2\rho U}{2}\int \frac{d^2\boldsymbol{x}d^2\boldsymbol{x}'}{A} v(\boldsymbol{x}-\boldsymbol{x}') \times |\psi(\boldsymbol{x})|^2|\psi(\boldsymbol{x}')|^2, \tag{2}$$

where A stands for the area of the system and $\psi(\boldsymbol{x})$ represents the normalized condensate wave function satisfying $\int dx|\psi(\boldsymbol{x})|^2 = A$. In these conditions, the local density of particles is given by $\rho(\boldsymbol{x}) = \rho|\psi(\boldsymbol{x})|^2$, where ρ corresponds to the dimensionless average density of particles. Additionally, the dimensionless parameter $U = V/\epsilon$ sizes the intensity of the pair interaction potential.

To investigate the ground state of the system, we minimize the energy per particle functional considering two complementary approaches. The first one uses a many-mode Fourier expansion for the wave function of the form [45,55]

$$\psi(\boldsymbol{x}) = \frac{c_0 + \frac{1}{2}\sum_{j\neq 0}^{j_{\max}} c_j \cos(\boldsymbol{k}_j\cdot\boldsymbol{x})}{\left(c_0^2 + \frac{1}{4}\sum_{j\neq 0}^{j_{\max}} c_j^2\right)^{1/2}}, \tag{3}$$

to determine the ground state configuration. The set of Fourier amplitudes $\{c_j\}$ and the characteristic wave vectors of the pattern defined by $\{\boldsymbol{k}_j\}$ are taken as variational parameters for the minimization process [56,57], however they are constrained to reproduce solutions with specific symmetries as we explain later. The limit of the sum $j_{\max}$ in Eq. (3) is only formal. The Fourier expansion for the ground state wave function in Eq. (3) considers a set of vectors $\{\mathbf{k}_j\}$ that is two dimensional and is constructed recursively, using n_c successive combinations of the extended wave vectors basis for each pattern. All periodic solutions were constructed using $n_c = 30$, while the quasiperiodic solution uses $n_c = 8$.

The procedure starts by defining the extended basis of wave vectors, which for a modulated pattern that has n-fold rotational symmetry, contains exactly n wave vectors of the form $\{\cos(2\pi i/n), \sin(2\pi i/n)\}$ with $i = 0, 1..., n-1$. To further proceed, we perform all available combinations of the vector basis to determine the second generation of wave vectors. The third generation of wave vectors is then obtained combining all vectors of the second generation with the vectors of the extended basis and so on. This results in a set of vectors that grows exponentially on each iteration. Due to the lack of periodicity of the quasicrystal solution, the number of independent Fourier amplitudes in this case grows much faster with each iteration than in any other periodic case. This particular choice for the n_c variable yields 255 amplitudes for the hexagonal pattern and 184 amplitudes for the dodecagonal quasicrystalline pattern. Such truncation criterion showed good convergence properties at all the $\lambda^2\rho U$ tested along the whole phase diagram presented.

For the periodic solutions, we considered a group of possible ansätze for the ground state wave function consistent with all modulated patterns reported in the literature for two and three-length scale potentials with the same properties considered here [44,58]. One of the advantages of projecting the ground state wave function into a Fourier basis is that it allows us to obtain an exact analytical expression for the functional energy per particle in terms of the Fourier amplitudes and characteristic wave vectors. To complement this approach and to check that the set of possible solutions considered in our variational calculations is complete, we also performed GPE simulations evolving in imaginary time [59]. The dimensionless GPE associated to our problem when evolved in imaginary-time τ takes the form

$$\frac{\partial\psi(\boldsymbol{x},\tau)}{\partial\tau} = \left[\frac{1}{2}\boldsymbol{\nabla}^2 - N\int d\boldsymbol{x}' v(\boldsymbol{x}-\boldsymbol{x}')|\psi(\boldsymbol{x}',\tau)|^2\right]\psi(\boldsymbol{x},\tau), \tag{4}$$

where the wave function $\psi(\boldsymbol{x},\tau)$ should be normalized to unity at each step. The convolution integral related to the non-local interaction potential is carried out in Fourier space. The numerical solution of the GPE was obtained using adaptive Runge–Kutta algorithms and the linear size of the simulation box was chosen as $L = 512k_0^{-1}$ with mesh $\delta r = 0.5k_0^{-1}$. In order to determine the phases present in our phase diagram we established a protocol in which we study the stationary configuration of the system departing from different initial conditions, with and without rotational symmetry. In general, we seed a portion of a given structure in the center of our simulation box and integrate the GPE for long enough times until observe convergence to the stationary state. In our case, we verified that the local texture developed by the model in all cases is consistent with the kind of modulated pattern considered in our momentum space variational approach.

A comparison of the real space stationary configurations produced by the two distinct mean-field methods can be observed in Fig. 2. The first row of the figure, corresponding to the quasicrystalline state at $\sigma = 0.97$ and $\lambda^2\rho U = 0.50$, display in (a) and (b) the results produced by the momentum space variational method and GPE simulations, respectively. Analogously, figures (c–d) show the stationary hexagonal decorated pattern obtained at $\sigma = 0.85$ and $\lambda^2\rho U = 1.00$. The density patterns produced by both methods agrees to an impressive level, not

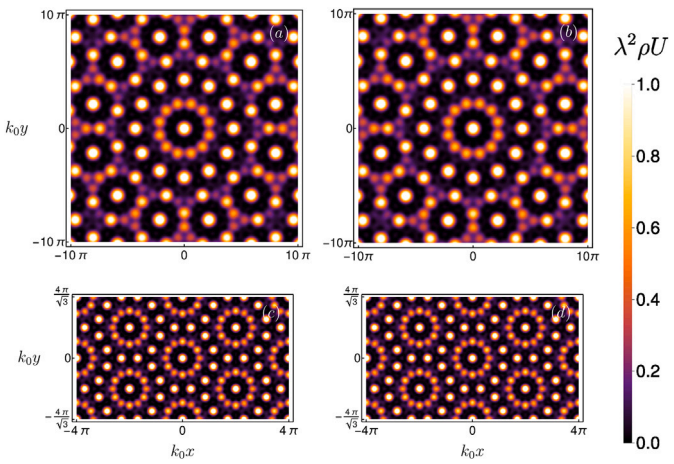

Fig. 2. Density plot comparison of the results from the momentum variational approach (first column) and GPE (second column). (a–b) corresponds to the quasicrystal configuration at $\sigma = 0.97$ and density $\lambda^2\rho U = 0.50$, while (c–d) corresponds to the decorated hexagonal pattern when $\sigma = 0.85$ and $\lambda^2\rho U = 1.00$.

only the aperiodic or periodic lattice of bigger cluster in both cases coincide, but also the intricate subdominant smaller cluster structure of the dodecagonal quasicrystal pattern. In spite of the density profile agreement, we observed that the energy values have a small relative error of 10^{-2}, with the variational method producing lower energies for moderate to low values of $\lambda^2\rho U$.

Additionally, we complement our study of the modulated phases by estimating the superfluid fraction (f_s) using the criterion provided by Legget [60]. Due to mathematical convenience, we take advantage of a recent result [45] showing that the original expression proposed by Legget for periodic and quasiperiodic patterns is equivalent to

$$f_s = \left(\int \frac{d^2\boldsymbol{x}}{A}|\psi(\boldsymbol{x})|^{-2}\right)^{-1}. \tag{5}$$

By including the characterization of the superfluid fraction in the phase diagram using GPE simulations, we can identify regions in which the modulated phases exist in a superfluid $(f_s > 10^{-2})$ or insulating state $(f_s < 10^{-2})$. Mean-field descriptions of condensate phases using Gross–Pitaevskii equation or its equivalents, like the variational theory employed, are not able to produce a strictly insulating phase $(f_s = 0)$.[2] For this reason, our superfluid-insulator transition is smoothed out by our calculation method. It is expected that beyond mean-field calculations, the appropriate description of the superfluid phase fluctuations could produce a strictly zero superfluidity for the insulating phase.

The specific threshold choice of the superfluid fraction proposed to differentiate superfluid and insulating states is in agreement with quantum Monte Carlo simulations for a related model [48]. This study shows that in the regime in which the mean-field calculations produces a low superfluid fraction of the order of 10^{-2}, PIMC calculations exhibit a phase transition to a strictly globally insulating state. Reasonable higher thresholds would produce a shift in the phase boundary without affecting our predictions regarding the existence of super-solid or super quasicrystal phases.

The behavior of the global superfluid fraction with respect to parameter $\lambda^2\rho U$ obtained using the variational approach (blue circles) and GPE simulations (orange diamonds) is shown in Fig. 3, for a specific value of the potential parameter $\sigma = 0.97$. It is possible to observe that the variational approach at moderate to high values of

[2] Since Gross–Pitaevskii equation can be cast as a Schrodinger equation, it also produces ground state wave functions with no nodes for finite interaction potentials.

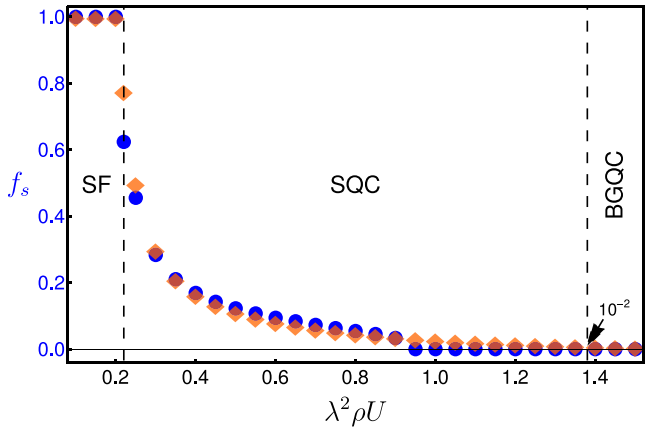

Fig. 3. Behavior of the superfluid fraction as the parameter $\lambda^2\rho U$ is increased for $\sigma = 0.97$. Blue circles corresponds to the variational approach in momentum space while orange diamonds refers to real space GPE simulations. (For interpretation of the references to color in this figure legend, the reader is referred to the web version of this article.)

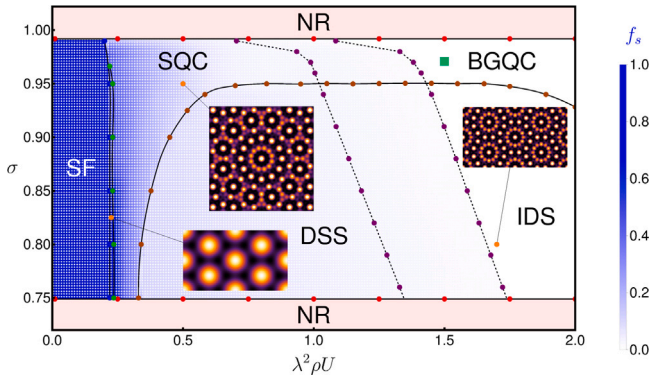

Fig. 4. Ground state phase diagram in the σ versus $\lambda^2\rho U$ plane. The small blue points with varying opacity represent the value (see legend) of the superfluid fraction at each point in the diagram. The non-relevant area (NR) corresponds to regions in which our LPG model is inconsistent with the constraints imposed to the potential. The right most dashed line with points in purple corresponds to the boundary of the phases with finite global superfluidity ($f_s \geq 10^{-2}$) following the criterion explained in the main text. The left most dashed line corresponds to $f_s = 3.0 \times 10^{-2}$ serving as a guide to the eyes for the slowly varying global superfluid fraction. The local properties of the green square are explored in Fig. 5(a)–(c).

$\lambda^2\rho U$ displays a spurious transition to a phase with strictly zero global superfluidity. This issue is related to the fact that in this regime the variational method produces a wave function that by a small amount is not strictly positive in the low local density regions between the cluster of particles. Moreover, this effect is produced by the truncation of the Fourier expansion in our ansätze for the ground state wave function at large values of $\lambda^2\rho U$. Although we consider a significant Fourier basis, to properly capture the behavior of the wave function in the depleted regions of the pattern and hence the value of f_s, a huge Fourier basis is required for the numerical calculations. While this issue affects the superfluid fraction, it does not have a strong impact on the energy values of a given pattern and in this sense, the ground state phase diagram is completely reliable. Due to this numerical difficulty, we decided to evaluate the superfluid fraction for the phase diagram in Fig. 4 using GPE simulations.

Phase diagram

The results of the variational mean-field method in combination with GPE simulations are shown in the ground state phase diagram of Fig. 4. The phase boundaries between the different phases – homogeneous, solids and quasicrystals – are determined from the direct minimization of our energy functional (2) using the variational mean-field method. Additionally, GPE simulations were performed to verify the stability of the modulated phases predicted by the mean-field technique and to study of the global and local superfluid properties. This study allow us to identify the globally superfluid $\left(f_s > 10^{-2}\right)$ and insulating phases $\left(f_s < 10^{-2}\right)$. The superfluid characterization implies that in the regions in which we have the coexistence of modulated phases and superfluidity, we have supersolid, or supersolid-like phases, while in the regions in which the modulated phases are concomitant with the absence of superfluidity, we have insulators, at least from the global perspective. However, as we will see shortly, the absence of global superfluidity does not rule out the existence of local superfluidity in certain ring structures of the modulated patterns. Here we can observe six distinct phases: the homogeneous superfluid phase (SF), a supersolid hexagonal phase, which is only stable for low enough values of σ in a quite narrow region of densities, a super dodecagonal quasicrystal (SQC), a supersolid decorated hexagonal phase (DSS), an insulating decorated solid (IDS) and a Bose glass quasicrystal (BGQC).

To better understand the nature of the insulating phases in our phase diagram, we now turn our attention to their local properties. In Fig. 5(a)–(c) we present a study of the ground state configuration at $\sigma = 0.97$ and density $\lambda^2\rho U = 1.50$, which corresponds to a value in Fig. 4 within the insulating BGQC (green square). Fig. 5(a) shows the density profile of the central region of the quasicrystal pattern. It is possible to observe how the structure is formed by a composition of different kinds of corona structures formed by twelve clusters of particles distributed over a circumference. The central coronas of the pattern were highlighted using white rings with radius $k_0 r = 2.19\pi, 4.27\pi$, and 6.19π, respectively.

To study the local superfluidity associated to the coronas structure, we employ again the Legget criterion considering the effective 1D system [61] defined by the density profile on the highlighted circumferences. In terms of the parametrized wave function $\varphi(\theta) = \psi(R\cos(\theta), R\sin(\theta))$, where R represent the radius of the circumference and θ represent the polar angle, the local superfluid fraction can be calculated as

$$f_l = \left(\int_0^{2\pi} \frac{d\theta}{2\pi} |\varphi(\theta)|^2 \times \int_0^{2\pi} \frac{d\theta}{2\pi} |\varphi(\theta)|^{-2} \right)^{-1}. \tag{6}$$

Here we have considered that since $N\psi^2(\mathbf{r})$ represents the local density of particles in the system, it is natural to evaluate the local superfluid fraction in the ring structure normalizing over this region the global wave function.[3]

In Fig. 5(b), we compute simultaneously the average density profile of the pattern in the radial direction and the normalized superfluid fraction corresponding to each of the highlighted central corona structures. The blue circles correspond to the superfluid fraction calculated using the density profile from the variational approach while the orange diamonds use the GPE simulation results. As we can observe both methods predict equivalent results for this quantity even in the insulating phases. This is a consequence that in regions with a significant density of particles the minimization variational method accurately describe the density profile since they contribute the most to the energy of the system. It is interesting to notice that while the global superfluid fraction obtained from both methods is effectively zero, we find a high value for the local superfluidity on the first and third corona structure, while the second one reproduces the behavior of the global superfluidity within the insulating regime.

Although not shown, a similar analysis in the decorated phase for the local superfluidity produces alike results, indicating that this kind

[3] See Eq.(16) of Ref. [61].

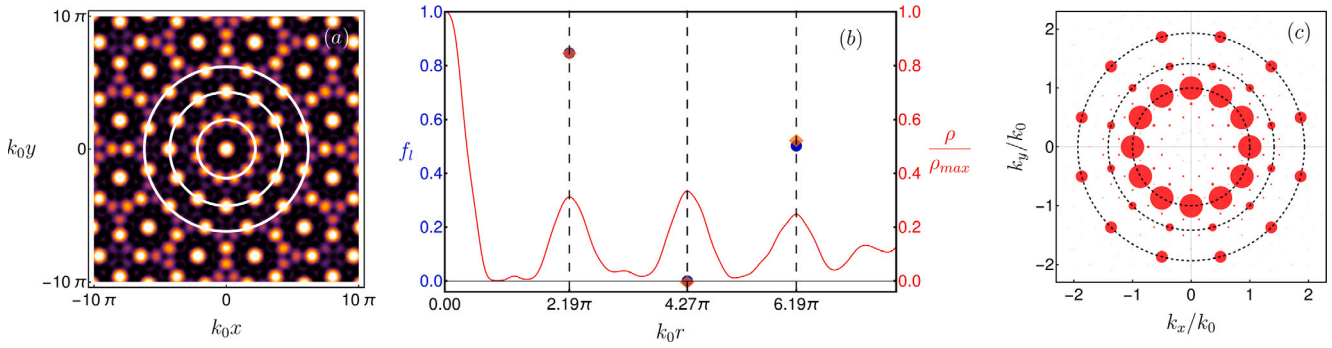

Fig. 5. (a) Real space density plot of the quasicrystalline structure in the insulating phase for the interaction potential parameter $\sigma = 0.97$ and density $\lambda^2\rho U = 1.50$ obtained from the variational approach. The three white rings represent the circles of interest at which we evaluate the local superfluid fraction of the system in (b). **(b)** Local superfluid fraction obtained for the white circles indicated in (a) using the variational approach (blue circles) and GPE simulations (orange diamonds). The red line indicates the average radial density. **(c)** Structure factor of the quasicrystalline structure at the same parameter values indicated in (a). Here the three black dashed circles represent the three minima structure of the LPG interaction potential at $\{k_0, \sqrt{2}k_0, \sqrt{3+\sqrt{2}}k_0\}$. (For interpretation of the references to color in this figure legend, the reader is referred to the web version of this article.)

of property in our case should be mostly associated with the kind of pair interaction potential we are considering and not exclusively with a particular phase. Indeed, the pair potential in our case punishes with a high energy cost all Fourier modes of the density pattern with characteristic wave vector $k \geq 2k_0$. In Fig. 5(c), we show the Fourier modes distribution for the density pattern in Fig. 5(a), where the radius of the circles are proportional to the absolute value of the corresponding Fourier amplitudes. As we can observe the main excited modes coincide with the minima of the interaction potential, signaled by the black dashed circumferences. Moreover, this also confirms that although present in our variational ansätze, modes with high momentum are in fact strongly suppressed, which should reflect in a large $\lambda^2\rho U$ extension of the regime hosting local but not global superfluid properties.

The phenomenology described above indicates that actually the quasicrystal insulating phase is a BGQC. In this context, the BGQC is characterized by two main properties: (i) the presence of local superfluidity on certain ring structures of the globally insulating quasicrystalline pattern and (ii) the existence of arbitrarily low energy particle-hole excitations in some of the regions hosting local superfluid properties. In these regions, the local potential experienced by each particle is quasi-disordered in the sense that it lacks periodicity from each of these ring structures to the others. The presence of quasi-disorder introduces "random" energy differences between the localized ground states of neighboring valleys in a given ring structure, which in turn produces particle-hole excitations, due to the hopping of particles, with an energy arbitrarily low for an infinite system [20,37,50,62].

The direct calculation of the excitation spectrum for the system at hand is not a simple task. However, in the limit of $U \to 0$ and $\lambda^2\rho \to \infty$, with $\lambda^2\rho U = \text{const.}$, quantum fluctuations are negligible and we can study single particle excitations as those of a free bosonic gas in the presence of a quasiperiodic effective external potential of the form $v_{\text{eff}}(\mathbf{x}) = \int d\mathbf{x}' v(\mathbf{x}-\mathbf{x}')|\psi_0(\mathbf{x}')|^2$, where $\psi_0(\mathbf{x})$ represents the ground state wave function. The properties of a free bosonic gas subjected to a 2D quasiperiodic potential have been recently considered in various works [63,64], showing that the single particle excitation spectrum has a fractal nature, with extended, critical and localized states depending on the depth of the external quasiperiodic lattice. By analogy, we can conclude that our model will also share these properties.

Additionally, it is worth noticing that our characterization of the BGQC phase does not take into account the behavior of the compressibility of the system, as it is usual [48,49], since by definition our model is always compressible. Furthermore, we would like to clarify that, independently of its superfluid properties, a decorated solid phase will always have a well-behaved energy spectrum formed by alternating bands and gaps, according to Bloch's theorem [65]. This behavior is incompatible with the fractal energy spectrum and localized states expected for a Bose glass, ruling out the occurrence of the latter within the region corresponding to the decorated solid. This can also be understood by noting that, for periodic solutions, particle-hole excitations within the ring structures will have the same finite excitation energies over the entire system.

Lastly, we would like to take a closer look at the validity of the mean-field picture presented above. On general grounds, according the Bogoliubov's theory for weakly interacting gases, the mean-field description is valid as long as the non-condensed fraction of the system is small, which usually implies weak enough interactions between particles to not expel a significant part of the system out of the condensate phase. In this framework the non-condensed fraction yields [66]

$$f_{nc} = \frac{1}{2\lambda^2\rho}\int \frac{d^2k}{(2\pi)^2}\left(\frac{t(k)+\lambda^2\rho U\hat{v}(k)}{\epsilon(k)} - 1\right), \tag{7}$$

where $t(k) = k^2/2$ and $\epsilon(k) = \sqrt{t(k)(t(k)+2\lambda^2\rho U\hat{v}(k))}$. Expression (7) can be used directly for $\lambda^2\rho U$ values below the roton instability boundary, when $\epsilon(k) > 0$ for all k. For higher values of $\lambda^2\rho U$, $\epsilon(k)$ develops a region taking imaginary values, which in our case signals an instability of the homogeneous towards the development of a modulated phase. Beyond the roton instability boundary, this expression can still be used imposing a proper integration cut-off excluding the momentum contribution where $\epsilon(k)$ is imaginary. This technique is well established for the determination of the condensate depletion or the Lee–Huang–Yang correction for quantum dipolar gases [67–69].

In this way, we proceed with the numerical evaluation of the non-condensed fraction for the pair interaction potential obtained at $\sigma = 0.97$ in the $\lambda^2\rho$ versus U plane. The results are presented in the density plot of Fig. 6 confirming the general expectation that f_{nc} is small for large $\lambda^2\rho$ and low U. The contours corresponding to $f_{nc} = 5\%$ and $f_{nc} = 10\%$ were highlighted as a guide to the eye for the region of validity of the mean-field results in the $\lambda^2\rho$-U plane. Moreover, the hyperbola $\lambda^2\rho U \approx 0.246$ marks the roton stability boundary, while $\lambda^2\rho U = 1.0, 2.0$ were only included as a reference to locate the region of parameters considered in the phase diagram presented in Fig. 4.

It is worth noticing that for the potential considered the value of $\lambda^2\rho$ needed to cross the limit of stability of the homogeneous phase, keeping $f_{nc} = 0.1$, is of the order of 60. To have an understanding of the meaning of this value, we could consider for instance a small portion of our quasicrystal containing the first three coronas of the system as depicted in (Fig. 5 a). The radius of the outer corona in this case is approximately 6π, this imply that a potential PIMC simulation of the system in this case would need more than 6×10^4 particles, only to reach the quasicrystal phase boundary. The ultimate conclusion of this analysis is that within the region of validity of the mean-field results (say $f_{nc} \leq 0.1$) the realization of PIMC simulations for

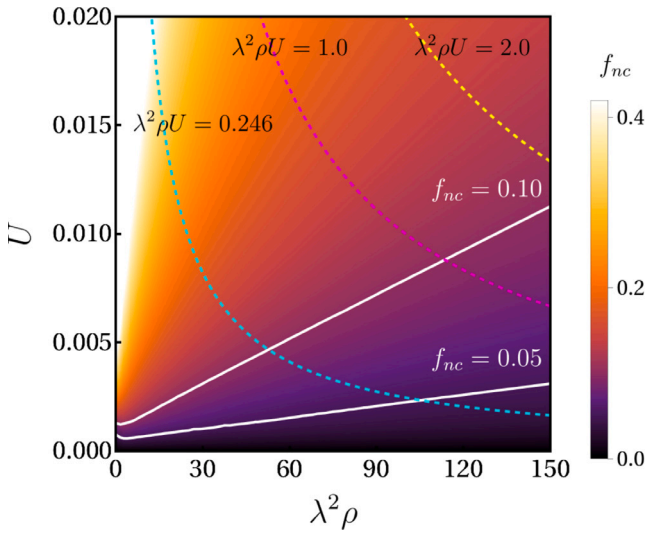

Fig. 6. Behavior of the non-condensed fraction (f_{nc}) of the homogeneous phase as the parameter $\lambda^2\rho$ and U are varied for $\sigma = 0.97$. The non-condensed fraction is determined within the Bogoliubov theory for weakly interacting gases. The light blue hyperbola $\lambda^2\rho U \approx 0.246$ corresponds to the roton stability boundary, beyond this value of $\lambda^2\rho U$ the non-condensed fraction is calculated introducing appropriate cut-off. See main text for details. (For interpretation of the references to color in this figure legend, the reader is referred to the web version of this article.)

the quasicrystal phase is completely out of reach considering that our current computational capabilities allow us to simulate systems with a few thousands particles.

PIMC simulations

In the present section we are going to probe the investigated system by means of a PIMC method. Such a technique allows us to obtain insightful information by performing simulations in the large U and low $\lambda^2\rho$ region. In this strongly correlated region, the values of the parameter $\lambda^2\rho U$ corresponding to the different phase boundaries are expected to be much different from those obtained within the mean-field approach. However, the possible verification of the existence of a self-sustained Bose glass phase, even in a region of parameters in which the mean-field description fails, would be a significant proof of concept of the realization of this novel phase.

In this way, we employ continuous-space PIMC method with the aid of the efficient worm algorithm to deeply investigate the proposed system [54]. In this form PIMC provides an accurate description of a quantum system by estimating the key thermodynamic observables. As known, the methodology works in a regime of finite temperature albeit a proper extrapolation to the T=0 limit has been correctly obtained in numerous systems [70]. In the present work, we simulate a system with a fixed number of quantum particles to obtain the particle density distribution and the local superfluid fraction. When addressing quasicrystalline geometries, periodic boundary conditions are not reliable and it is preferred to use external confinement [71,72]. In this case, we employed an external potential of the form $V(r) \propto (r/r_c)^\alpha$ with α a large integer e.g. $\alpha = 30$ and $r_c = 30$, a large enough value to contain the first four coronas; this approximates an infinite wall at r_c. Both the external potential and the interaction (1) are included in the density matrix through the primitive approximation [53].

In order to confirm the stability of the structures seen in the mean-field methods, and to evidence deviations, we perform simulations in continuous space starting from a density profile derived from the mean-field ground state. The starting configuration is derived as follows. First, we select a portion of the ground state, as a circle of radius R centered in the symmetry center of the quasicrystal. We pick a density n, and from it, we derive the particle number as $N = n/\pi R^2$. Inside the circle, we use a thresholding algorithm to determine regions of high density, corresponding to the clusters forming the quasicrystal structure. To each cluster j, we assign a weight w_j, proportional to the integrated density on the cluster; a number of particles N_j are then assigned to each cluster proportionally to w_j, approximating them so that each cluster has an integer number of particles. Finally, the particles are positioned randomly within each cluster, proportionately to the density. The goal of this process is to ensure that different clusters have a balanced number of particles, without introducing strong fluctuations of the particle number in the clusters. In particular, on our simulations we use $N = 2000$ and $2mk_BT/\hbar^2k_0^2 = 1$.

In a finite system, information about the superfluid fraction is provided by the area estimator [53,73,74]. The original formulation has been extended to describe the local profile of the superfluid density [75], which can be used to estimate the superfluid fraction in finite regions [71,72]. For the problem at hand, this allows us to verify the mean-field results about local superfluidity in the coronas. This observable is evaluated by dividing the system into a finite number of concentric regions ($k = 1, 2, \ldots, K$) and then defining the superfluid fraction for the kth zone as follows

$$f_{s,k} = \frac{1}{I_{cl,k}} \int_k \rho_s(\mathbf{r})\, r^2 d\mathbf{r}\,, \tag{8}$$

where $I_{cl,k}$ represents classical moment of inertia related to the zone k. This term is defined in a way that $I_{cl} = \sum_{k=1}^{K} I_{cl,k}$ results the total moment of inertia. Regarding the estimation of superfluidity as defined in Eq. (8), the PIMC method has to evaluate the radial superfluid density, $\rho_s(\mathbf{r})$. This is done by employing the so-called area estimators. So the complete form of $\rho_s(\mathbf{r})$ reads

$$\rho_s(\mathbf{r}) = \frac{4}{\beta} \frac{\langle A_z A_z(\mathbf{r})\rangle - \langle A_z\rangle\langle A_z(\mathbf{r})\rangle}{r^2}\,. \tag{9}$$

$\langle\cdots\rangle$ denoting the statistical mean values of an observable. A_z is the component of the total area enclosed by particle paths on the xy-plane

$$A_z = \frac{1}{2}\sum_{i=1}^{N}\sum_{m=0}^{M-1} \left(\mathbf{r}_i^m \times \mathbf{r}_i^{m+1}\right)_z\,, \tag{10}$$

M being the number of time slices employed over a simulation, while $\mathbf{r}_i^m$ represents the particle's bead i in the mth position [53,73]. The spatially dependent A_z reads

$$A_z(\mathbf{r}) = \frac{1}{2}\sum_{i=1}^{N}\sum_{m=0}^{M-1} \mathbf{r} \times \mathbf{r}_i^{m+1}\delta(\mathbf{r} - \mathbf{r}_i^m)\,. \tag{11}$$

As shown in Fig. 7(a–c), we were able to distinguish a superfluid, insulating, and Bose glass phase, similar to what is shown in Ref. [71]. Briefly, the three phases are identified by measuring two zonal quantities in different coronas: the superfluid fraction, and the fluctuation in particle number (zonal compressibility). A superfluid phase is characterized by finite values of both zonal superfluid fraction and zonal compressibility in all coronas. Similarly, an insulating phase is characterized by a null value of both quantities in all coronas: no superfluid response is present, and localized particles cannot jump from one corona to another, therefore there are no fluctuations in particle number. Finally, a Bose glass is characterized by an intermediate regime: particles are again localized, leading to vanishing fluctuations in particle number, but the zonal superfluid fraction is finite in one or more of the coronas. This is a signature of the locally superfluid puddles that characterize a Bose glass phase. For a choice of parameters, we observe a transition of the same kind as seen in mean-field, except that the transition from insulator to Bose glass is shifted to much smaller values of $\lambda^2\rho U$, e.g. $\lambda^2\rho U \approx 0.02$ for $\sigma = 0.97$. An example of the behavior of the local superfluidity in the different coronas withing the Bose glass phase is shown in Fig. 7(d). As we can observe the local superfluid properties obtained in simulations are qualitatively

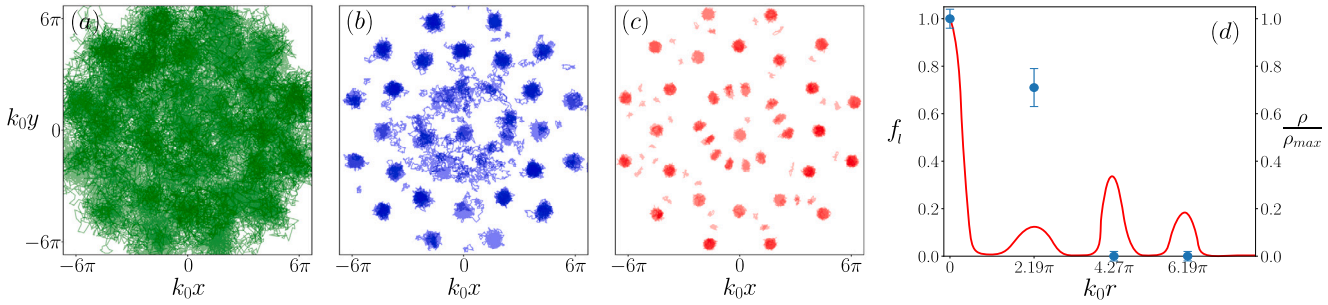

Fig. 7. **(a–c)** PIMC world line configurations, for the superfluid **(a)**, Bose glass **(b)**, and insulating phase **(c)**. The strengths of the interaction potential were selected as $U = 0.016$ (a), $U = 0.032$ (b) and $U = 0.32$ (c), while the density was held fixed at $\lambda^2\rho \approx 0.71$. **(d)** Normalized radial density distribution in the Bose glass phase (red solid line) and zonal superfluidity in the coronas (blue circles). (For interpretation of the references to color in this figure legend, the reader is referred to the web version of this article.)

the same to those reported in the mean-field study. The insulating behavior displayed by the last corona of the simulated system is already expected due the absence of the subsequent quasicrystal structure in the simulations.

It is interesting to notice how in the low $\lambda^2\rho$ and high U regime the system freezes at a much lower value of $\lambda^2\rho U$. This is an indicative that in these conditions correlations plays a major role in the behavior of the system, in contrast to the mean-field behavior. Other minor effects that could also contribute for the difference observed in the occurrence of the QC phase transition is the lack of the frustration produced by the external part of the quasicrystal, not present due to the finite size of the simulated system. Finally, we would like to note that although the PIMC simulations available with our current computational capabilities are still very far from the mean-field regime, it is remarkable that they have confirmed the sequence of phases predicted by the mean-field analysis, particularly the existence of a self-assembled Bose glass phase, proposed in this work by the first time.

Conclusions and discussion

In the present work, we studied the ground state properties of a two-dimensional bosonic gas interacting via a LPG pair potential. The selected model presents three characteristic length scales properly chosen in order to favor the stabilization of a dodecagonal quasicrystal structure. The phase diagram of the system is investigated using two mean-field complementary methods. The first one follows a direct variational approach to determine the optimal modulated ground state, given as an expansion in Fourier modes for each kind of modulated solution. To test and complement these results we perform extensive Gross–Pitaevskii simulations along the phase diagram. While the first variational method was employed to construct the modulations phase diagram, Gross–Pitaevskii simulations were used to obtain an accurate description of the superfluid properties deep into the modulated region of the phase diagram. Additionally, we performed PIMC simulations of a restricted region of the quasicrystal structure to verify the presence of a Bose glass phase as well as the stability of the self-induced quasicrystal structure.

Our results shows that for high enough $\lambda^2\rho U$ values the self-induced quasicrystal phase eventually lose its global superfluid properties. However, in this regime it is able to host local superfluidity in certain rings structures of the quasiperiodic pattern. This kind of behavior is taken as a signature of a Bose glass phase, considering that in the present system, due to absence of a rigid lattice, compressibility will be always finite. The main ingredient for the phenomenology reported is the presence of a pair interaction with the adequate three minima structure in momentum space, which is currently within experimental reach [26–31]. Additionally, PIMC simulations confirmed qualitatively the scenario obtained from the mean-field study. Within both methods, the first corona of the quasicrystalline pattern is able to retain superfluidity while the second corona of the structure mirrors the global insulating behavior. Finally, we believe that the results presented in this work motivates new experiments in the direction of producing a self-induced quasicrystal phase. Not only due to the exotic nature of such a phase but also due to the possibility of an eventual production of the elusive Bose glass phase.

CRediT authorship contribution statement

M. Grossklags: Writing – review & editing, Writing – original draft, Validation, Software, Methodology, Investigation, Data curation, Conceptualization. **M. Ciardi:** Writing – review & editing, Writing – original draft, Software, Investigation, Data curation, Conceptualization. **V. Zampronio:** Writing – review & editing, Writing – original draft, Software, Investigation. **F. Cinti:** Writing – review & editing, Writing – original draft, Supervision, Resources, Funding acquisition, Conceptualization. **A. Mendoza-Coto:** Writing – review & editing, Writing – original draft, Supervision, Methodology, Investigation, Conceptualization.

Declaration of competing interest

The authors declare the following financial interests/personal relationships which may be considered as potential competing interests: Alejandro Mendoza-Coto reports financial support was provided by Max-Planck-Institute for the Physics of Complex Systems. If there are other authors, they declare that they have no known competing financial interests or personal relationships that could have appeared to influence the work reported in this paper.

Data availability

Data will be made available on request.

Acknowledgments

We thank the NICIS-CHPC agency for providing computational resources. A.M.C. acknowledges Fundação de Amparo à Pesquisa de Santa Catarina, Brazil (FAPESC) and Max Planck Institute for the Physics of Complex Systems (MPIPKS) for financial support. V.Z. M.C. and F.C. acknowledge financial support from PNRR MUR Project No. PE0000023-NQSTI.

References

[1] Seul M, Andelman D. Science 1995;267(5197):476–83.
[2] Andelman D, Rosensweig RE. J Phys Chem B 2009;113(12):3785–98.
[3] Mendoza-Coto A, Stariolo DA, Nicolao L. Phys Rev Lett 2015;114:116101.
[4] Mendoza-Coto A, Nicolao L, Díaz-Méndez R. Sci Rep 2019;9(1):2020.
[5] Likos CN. Phys Rep 2001;348:267–439.
[6] Zhang R, Mozaffari A, de Pablo JJ. Nat Rev Mater 2021;6(5):437–53.
[7] Andreev AF, Lifshitz IM. Sov Phys Jetp-USSR 1969;29(6):1107.
[8] Chester GV. Phys Rev A 1970;2:256–8.
[9] Kim E, Chan MHW. Nature 2004/01/01;427(6971):225–7.

[10] Cinti F, Jain P, Boninsegni M, Micheli A, Zoller P, Pupillo G. Phys Rev Lett 2010;105(13):135301.
[11] Boninsegni M, Prokof'ev NV. Rev Modern Phys 2012;84:759–76.
[12] Cinti F, Macrì T, Lechner W, Pupillo G, Pohl T. Nature Commun 2014/02/04/online;5:3235 EP.
[13] Ciardi M, Cinti F, Pellicane G, Prestipino S. Phys Rev Lett 2024;132:026001.
[14] Cinti F. Phys Rev B 2019;100:214515.
[15] Pupillo G, Ziherl P, Cinti F. Phys Rev B 2020;101:134522.
[16] Madison KW, Chevy F, Wohlleben W, Dalibard J. Phys Rev Lett 2000;84:806–9.
[17] Tsubota M, Kasamatsu K, Ueda M. Phys Rev A 2002;65:023603.
[18] Abo-Shaeer JR, Raman C, Vogels JM, Ketterle W. Science 2001;292(5516):476–9.
[19] Henkel N, Cinti F, Jain P, Pupillo G, Pohl T. Phys Rev Lett 2012;108:265301.
[20] Fisher MPA, Weichman PB, Grinstein G, Fisher DS. Phys Rev B 1989;40:546–70.
[21] Krauth W, Trivedi N, Ceperley D. Phys Rev Lett 1991;67:2307–10.
[22] Scalettar RT, Batrouni GG, Zimanyi GT. Phys Rev Lett 1991;66:3144–7.
[23] Damski B, Zakrzewski J, Santos L, Zoller P, Lewenstein M. Phys Rev Lett 2003;91:080403.
[24] Fallani L, Lye JE, Guarrera V, Fort C, Inguscio M. Phys Rev Lett 2007;98:130404.
[25] Boninsegni M, Prokof'ev N, Svistunov B. Phys Rev Lett 2006;96:105301.
[26] Mivehvar F, Piazza F, Donner T, Ritsch H. Adv Phys 2021;70(1):1–153.
[27] Karpov P, Piazza F. Phys Rev Lett 2022;128:103201.
[28] Vaidya VD, Guo Y, Kroeze RM, Ballantine KE, Kollár AJ, Keeling J, et al. Phys Rev X 2018;8:011002.
[29] Gopalakrishnan S, Lev BL, Goldbart PM. Nat Phys 2009;5(11):845–50.
[30] Gopalakrishnan S, Lev BL, Goldbart PM. Phys Rev A 2010;82:043612.
[31] Zhang Y-C, Walther V, Pohl T. Phys Rev A 2021;103:023308.
[32] Greiner M, Mandel O, Esslinger T, Haensch T, Bloch I. Nature 2002;415:39–44.
[33] Mendoza-Coto A, Stariolo DA. Phys Rev E 2012;86:051130.
[34] Barci DG, Mendoza-Coto A, Stariolo DA. Phys Rev E 2013;88:062140.
[35] Mendoza-Coto A, Barci DG, Stariolo DA. Phys Rev B 2017;95:144209.
[36] Mendoza-Coto A, de Oliveira DEB, Nicolao L, Díaz-Méndez R. Phys Rev B 2020;101:174438.
[37] Fallani L, Lye JE, Guarrera V, Fort C, Inguscio M. Phys Rev Lett 2007;98:130404.
[38] Shechtman D, Blech I, Gratias D, Cahn JW. Phys Rev Lett 1984;53:1951–3.
[39] Levine D, Steinhardt PJ. Phys Rev B 1986;34:596–616.
[40] Senechal M. Quasicrystals and geometry. Cambridge University Press; 1996.
[41] Lifshitz R, Diamant H. Phil Mag 2007;87(18–21):3021–30.
[42] Dotera T. Isr J Chem 2011;51(11–12):1197–205.
[43] Barkan K, Diamant H, Lifshitz R. Phys Rev B 2011;83:172201.
[44] Barkan K, Engel M, Lifshitz R. Phys Rev Lett 2014;113:098304.
[45] Mendoza-Coto A, Turcati R, Zampronio V, Díaz-Méndez R, Macrì T, Cinti F. Phys Rev B 2022;105:134521.
[46] Yao H, Khoudli A, Bresque L, Sanchez-Palencia L. Phys Rev Lett 2019;123:070405.
[47] Yao H, Giamarchi T, Sanchez-Palencia L. Phys Rev Lett 2020;125:060401.
[48] Gautier R, Yao H, Sanchez-Palencia L. Phys Rev Lett 2021;126:110401.
[49] Ciardi M, Angelone A, Mezzacapo F, Cinti F. Phys Rev Lett 2023;131:173402.
[50] Svistunov B, Babaev E, Prokof'ev N. Superfluid states of matter. Taylor & Francis; 2015.
[51] Pitaevskii LP. Sov Phys—JETP 1961;13(2):451–4.
[52] Gross EP. J Math Phys 1963;4(2):195–207.
[53] Ceperley DM. Rev Modern Phys 1995;67:279–355.
[54] Boninsegni M, Prokof'ev NV, Svistunov BV. Phys Rev E 2006;74(3):036701.
[55] Zhang Y-C, Maucher F, Pohl T. Phys Rev Lett 2019;123:015301.
[56] Prestipino S, Sergi A, Bruno E. Phys Rev B 2018;98:104104.
[57] Prestipino S, Sergi A, Bruno E. J Phys A 2019;52:015002.
[58] Lifshitz R, Petrich DM. Phys Rev Lett 1997;79:1261–4.
[59] Dennis GR, Hope JJ, Johnsson MT. Comput Phys Comm 2013;184(1):201–8.
[60] Leggett AJ. Phys Rev Lett 1970;25:1543–6.
[61] Sepúlveda N, Josserand C, Rica S. Phys Rev B 2008;77:054513.
[62] Jaksch D, Bruder C, Cirac JI, Gardiner CW, Zoller P. Phys Rev Lett 1998;81:3108–11.
[63] Zhu Z, Yu S, Johnstone D, Sanchez-Palencia L. Localization and spectral structure in two-dimensional quasicrystal potentials. 2023, arXiv:2307.09527.
[64] Zhu Z, Yao H, Sanchez-Palencia L. Phys Rev Lett 2023;130:220402.
[65] Bloch F. Zeitschrift für Physik 1929;52(7):555–600.
[66] Pitaevskii L, Stringari S. Bose-Einstein condensation and superfluidity (International series of monographs on physics book 164). OUP Oxford; 2016.
[67] Lima ARP, Pelster A. Phys Rev A 2012;86:063609.
[68] Saito H. J Phys Soc Japan 2016;85(5):053001. http://dx.doi.org/10.7566/JPSJ.85.053001.
[69] Bisset RN, Wilson RM, Baillie D, Blakie PB. Phys Rev A 2016;94:033619.
[70] Pollet L. Rep Progr Phys 2012;75(9):094501.
[71] Ciardi M, Macrì T, Cinti F. Phys Rev A 2022;105:L011301.
[72] Ciardi M, Macrì T, Cinti F. Entropy 2022;24(2).
[73] Sindzingre P, Klein ML, Ceperley DM. Phys Rev Lett 1989;63(15):1601–4.
[74] Zeng T, Roy P. Rep Progr Phys 2014;77(4):046601.
[75] Kwon Y, Paesani F, Whaley KB. Phys Rev B 2006;74:174522.